17th World Conference on Earthquake Engineering, 17WCEE
Sendai, Japan - September 13th to 18th 2020

EXPERIMENTS FOR VALIDATION OF FSI MODELS FOR SEISMIC RESPONSE OF ADVANCED REACTOR INTERNALS

F.U.H Mir[(1)], C.-C.Yu[(2)], A.S. Whittaker[(3)]

[(1)] *Ph.D. Candidate, Department of Civil, Structural, and Environmental Engineering, University at Buffalo, Buffalo, NY 14260, USA (faizanul@buffalo.edu)*
[(2)] *Ph.D. Candidate, Department of Civil, Structural, and Environmental Engineering, University at Buffalo, Buffalo, NY 14260, USA (cyu23@buffalo.edu)*
[(3)] *SUNY Distinguished Professor, Department of Civil, Structural, and Environmental Engineering, University at Buffalo, Buffalo, NY 14260, USA (awhittak@buffalo.edu)*

Abstract

Accurate prediction of the dynamic seismic response of reactor vessel internals (RVIs) submerged in fluid will be critical to the design, qualification and risk assessment of advanced nuclear reactors. Analytical solutions for submerged components using the incompressible inviscid theory or the more complicated compressible inviscid or incompressible viscous theories are available for simple geometrical shapes, idealized boundary conditions and unidirectional seismic inputs of small amplitude. The geometries and boundary conditions proposed for advanced reactors and their internals are complex and analytical solutions are generally not applicable. Physical testing of reactor vessels and internals is not feasible given their size and cost. Design, qualification and risk assessment calculations will have to rely on the use of verified and validated numerical models that are capable of capturing the interaction of internals with the surrounding fluid (fluid-structure interaction: FSI) over a wide range of shaking. A two-phase experimental program was performed on a six degrees-of-freedom earthquake simulator at the University at Buffalo to generate data that will support validation of numerical models in commercial finite element codes. Phase-I testing involved a model of a base-supported reactor vessel without head or internals. The focus of this paper is Phase-II testing that involved the Phase-I vessel with a head and internals. Phase-II experiments investigated pressure histories on reactor internals; added mass, added damping and coupling effects in internals along with strain and acceleration responses under three-component seismic excitations. The effects of seismic isolation on the dynamic responses of internals were investigated using numerically generated input motions simulating a virtual isolation system. The generated data will be curated and archived at the end of the testing program for later use by other analysts seeking to validate numerical models not evaluated by the authors.

Keywords: fluid-structure interaction, reactor internals, seismic qualification, seismic isolation

1. Introduction

Dynamic analysis is necessary to ensure that components essential to the safe operation and shutdown of a nuclear power plant remain functional in the design basis shaking. Many such components are submerged in fluid and their seismic interaction must be characterized. One example is shown in Figure 1: mechanical systems inside a liquid metal reactor [1]. Analytical solutions for submerged components using the incompressible inviscid theory or the more complicated compressible inviscid or incompressible viscous theories are available for simple geometrical shapes, idealized boundary conditions and unidirectional seismic inputs of small amplitude. However, the geometries, boundary conditions and configurations of advanced reactors and their internals are complex and analytical solutions are unavailable. Physical testing of reactor vessels and internals is not feasible given their size and cost. The design, qualification and risk assessment of advanced reactors are their internals will have to be based on analysis of verified and validated numerical models that are capable of capturing the interactions of internals with the surrounding fluid (fluid-structure interaction: FSI) and vessel over a wide range of three-component earthquake shaking.

A two-phase experimental program has been completed on a six degrees-of-freedom earthquake simulator at the University at Buffalo to generate data to support validation of numerical models in commercial finite element codes and demonstrate the utility of seismic isolation of equipment inside reactor buildings. The Phase-I testing involved a model of a base-supported reactor vessel with neither a head nor internals. Preliminary details of this program can be found in [2] and [3]. This paper introduces the Phase-II testing that involved the Phase-I vessel equipped with a head and internals. The Phase-II experiments investigated pressure histories on reactor internals, and added mass, added damping and coupling effects on internals along with strain and acceleration responses under three-component seismic excitations. The impact of seismic isolation on the coupled response of the vessel, its contained fluid, and internals was investigated using numerically generated input motions simulating a virtual isolation system. The Phase II tests are grouped into four series: Test series 1 through 4 (referred to as Test 1 through Test 4 hereafter). The following sections describe the four test specimens, the instrumentation and the seismic inputs used, and present sample, preliminary results from system-identification tests and earthquake-simulator tests.

The data generated from these tests will be used for validation of numerical models (some of which have been verified previously; see [4], [5] and [6]) for fluid-structure interaction in finite element codes and to identify the benefits of seismic isolation on the response of equipment in advanced reactors. The data from the experimental program will be made available on DesignSafe [7] for future use by others.

2. Specimens for Phase II testing

The specimens, instrumentation used, and objectives for each test are presented in this section.

2.1 Test 1

Test 1 involves a 1/10th scale model of a base-supported vessel that represents a liquid metal reactor at scale (see [2], [3]). The specimen was tested in two configurations, A and B. In configuration A, the water height was 1.62 m, with a freeboard of 0.41 m, and sloshing was permitted. In configuration B, the top of the vessel was sealed and the vessel was completely filled, thereby preventing sloshing. Earthquake motions consistent with fixed base (*non-isolated*) and *isolated* conditions were input with an objective of generating pressure, wave height (only in configuration A), base shear and base moment histories for the two conditions. Figure 2 shows the configuration A specimen installed on the earthquake simulator. Instrumentation used for Test 1 included twelve pressure gages installed on the wall of the vessel, four five-degrees-of-freedom load cells installed below the base of the vessel, accelerometers installed on the wall and base of the vessel, and in configuration A only, four float-and-Temposonic based wave height sensors [2, 3].

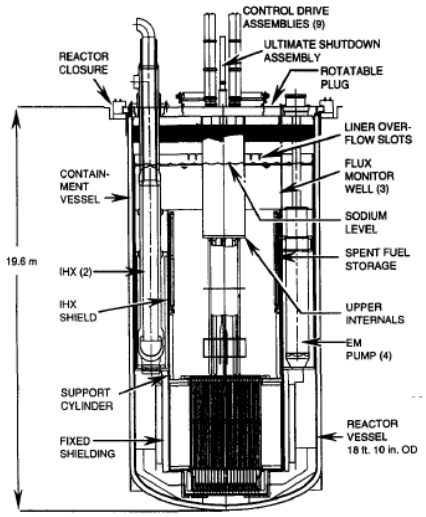

Figure 1. Reactor system [1]

Figure 2. Test 1, configuration A specimen

2.2 Test 2

Test 2 involved the Test 1 specimen together with a centrally placed steel tube internal (0.32 m outer diameter, 1.52 m long, and 6.4 mm wall thickness) tested in two configurations (A and B) as shown in Figure 3a and Figure 3b. The vessel is not shown in these photographs. The base of the central internal was sealed to prevent the ingress of water. Configuration B involves two aluminum tubes (0.15 m outer diameter, 0.9 m long, and 3.2 mm thick) to function as *baffles*, placed to the north and south of the central internal, as shown in Figure 3c. The primary objective of Test 2 was to generate pressure histories on the wall of the central internal and wave height histories for the two configurations subjected to *non-isolated* and *isolated* seismic inputs. The effect of the *baffles* on wave height, if any, will be investigated using the generated data. The instrumentation used for Test 2 was similar to that for Test 1. Hydrodynamic pressure on the wall of the central internal was recorded using three pressure gages (removed from the wall of the vessel). Three directional acceleration response was measured near the end of the central internal, at the ends of the two aluminum baffles (in configuration B) and at the center of the vessel head.

a. configuration A

b. configuration B

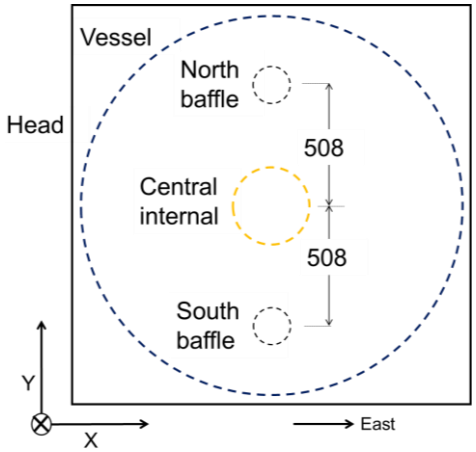

c. configuration B, plan view

Figure 3. Test 2 specimen, configurations A and B, dimensions in mm

2.3 Test 3

Test 3 involved a 1.83 m long steel plate internal, 12 mm × 150 mm in cross section (Figure 4a), placed at two different distances from the vessel wall, in two test configurations, as shown in Figure 4b and Figure 4c. The objective of Test 3 was to study added mass and damping effects for the plate in the two configurations and generate acceleration and strain response histories for the plate with the vessel, subjected to *non-isolated* and *isolated* inputs. In addition to the Test 1 instrumentation, two tri-axial accelerometers were installed at the bottom and mid-height of the plate and two strain gages were installed near its point of attachment to the vessel head.

a. plate internal and vessel head

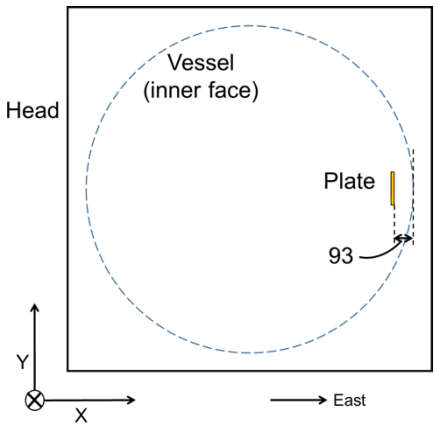

a. configuration A, plan view

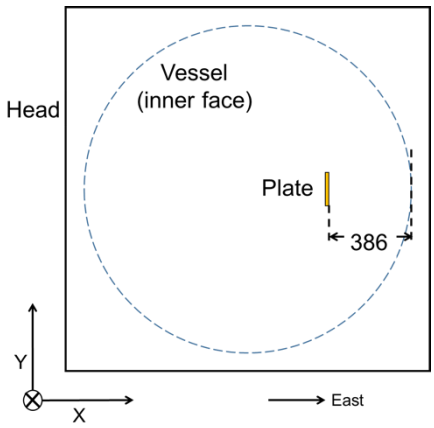

b. configuration B, plan view

Figure 4. Test 3 specimen, configurations A and B, dimensions in mm

2.4 Test 4

Test 4 involved two 1.83 m long aluminum tubular internals with diameters of 76 mm and 152 mm, tested in three configurations. Three specimens were fabricated; see Figure 5a. The wall thickness for the 76 mm and the 152 mm diameter internals was 1.7 mm and 3.2 mm, respectively, and steel discs weighing 4.82 kg and 9.88 kg, respectively, were attached at their ends (Figure 5b) to enable adjustment (reduction) of their natural frequencies. The three test configurations are shown in Figure 6a through Figure 6c. The objective of Test 4 was to study added mass, added damping and coupling effects for the internals and, as in case of Test 3, to generate acceleration and strain response histories for the internals with the vessel subjected to *non-isolated* and *isolated* inputs. The instrumentation of the vessel and its head for Test 4 was identical to that of Test 2. Two tri-axial accelerometers and two strain gages were installed on each internal.

a. internals for Test 4

b. weight attached at the end of an internal

Figure 5. Specimens for Test 4

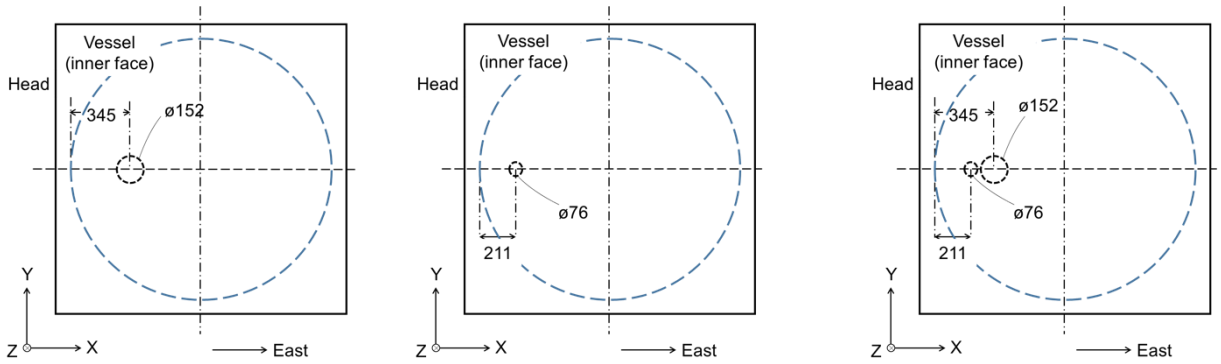

a. configuration A b. configuration B c. configuration C

Figure 6. Test 4, configurations A, B and C, dimensions in mm

3. Seismic inputs

Three recorded ground motions, time scaled to be consistent with the 1/10th length scale vessel, were used for earthquake-simulator testing. Five-percent damped response spectra of the *x*-components of the time-scaled motions are shown in Figure 7, amplitude scaled to a peak ground acceleration (PGA) of 1g. The horizontal components of the three time-scaled earthquake motions have different frequency contents: low for the Chi-Chi earthquake (CCE) to drive response in the isolated condition, and high for the El Centro (ECE) and Kern County (KCE) earthquakes. The maximum *x*-component PGA used for testing for each motion was determined on the basis of the available freeboard (with a goal of not sloshing water from the vessel) and the displacement capacity of the simulator's horizontal actuators.

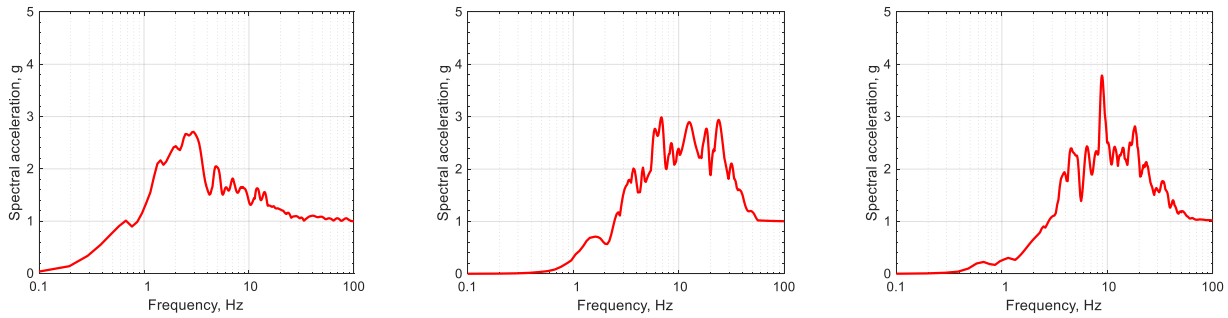

a. CCE b. ECE c. KCE

Figure 7. Response spectra of *x*-components of input motions used, PGA = 1.0 g, damping ratio of 5%

3.1 Generation of *isolated* motions

Simplified models were created in SAP2000 [8] to generate the *isolated* motions. The impulsive and convective modes were represented by two de-coupled oscillators [9] having infinite stiffness in the vertical direction. The vessel, head and the steel internal were assumed to be rigid and were modeled using lumped masses and rigid links. The mass of the steel plate (Test 3) and the aluminum baffle and internals (Test 2 and Test 4) was neglected. Four lumped-mass stick models, as shown in Figure 8, were considered: 1) Test 1 configuration A, 2) Test 1 configuration B, 3) Test 2, and 4) Test 3 (or 4). The impulsive and convective modes were characterized identically in models 1, 3 and 4. All of the fluid mass was modeled as impulsive in model 2 [10].

Three isolation systems (IS#1, IS#2 and IS#3), with sliding periods of 0.7 sec, 1 sec and 1.3 sec, were designed for the four models using Friction Pendulum™ isolators, which were modelled using link elements. The chosen periods correspond to typical values at the prototype (full) scale. The properties of the isolators in the four models were varied because the masses were different: see Figure 8. The isolator properties used for the three isolation systems in model 1 are listed in Table 1. Isolator properties for other three models are not shown here for conciseness. For each model and isolation system, a set of unidirectional, bi-directional and three-directional analyses was performed and the acceleration history at a point above the isolation system was recorded. These histories were used as inputs to the test specimens to simulate different isolation systems, that is, the *isolated* motions.

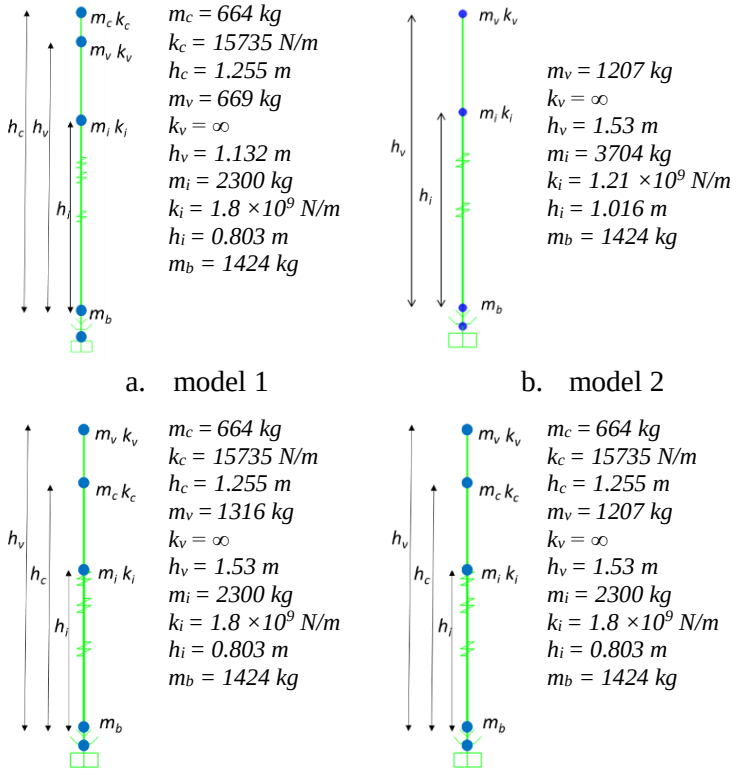

Figure 8. SAP models for generation of *isolated* motions

Table 1. Isolator properties used for used for model 1

System name	IS#1	IS#2	IS#3
Period, sec	0.7	1.0	1.3
Total weight, N	49609	49609	49609
Pendulum radius, m	0.122	0.248	0.419
Friction coefficient (fast)	0.06	0.06	0.06
Friction coefficient (slow)	0.03	0.03	0.03
Yield displacement, mm	1	1	1
Post-elastic stiffness, N/m	406631	200036	118398
Elastic stiffness, N/m	2976540	2976540	2976540

Five-percent damped response spectra for the *x*-component of input motions and their *isolated* counterparts for IS#1 and model 1 are shown in Figure 9. Two ranges on the *y*-axis are used. Figure 8a (CCE) shows amplification in spectral acceleration for frequencies between 1 Hz and 6 Hz, which is attributed to the low amplitude of the input for which the isolators do not slide appreciably. The effects of seismic isolation in

reducing the spectral accelerations for frequencies greater than approximately 2.5 Hz are evident in Figure 9b and Figure 9c. There is an increase in spectral demand between 1 Hz and 2 Hz for the isolated condition, in Figures 8b and 8c, that could lead to an amplified convective response as noted previously [11].

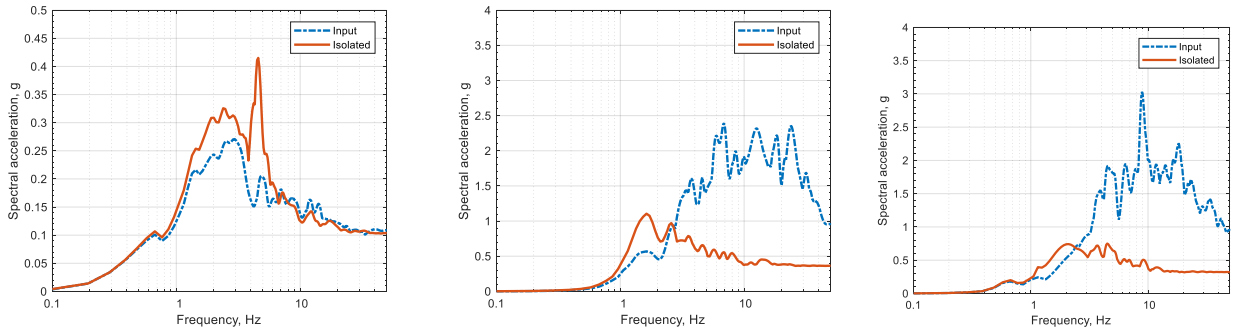

a. CCE b. ECE c. KCE

Figure 9. Response spectra of input and *isolated* motions for IS#1 in SAP model 1, 5% damping

4. System identification tests

Prior to the earthquake simulator tests, a series of impact tests was performed to characterize the *in-air* frequencies of the internals (Test 2 and Test 4), baffles (Test 2), and the plate (Test 3). For this purpose, the component was inverted and attached to the top of head, as shown in Figure 10a, and hit with an impact hammer. (The vessel was empty.) For the central steel internal of Test 2, an additional hammer test was conducted with its base bolted to the earthquake simulator platform as shown in Figure 10b. A comparison of natural frequencies estimated from the impact tests with those predicted using finite element (FE) models in LS-DYNA [12] is presented in Table 2. The test results are close to those predicted by the FE models for all components except the central steel internal, for which the measured frequency is 36% less than predicted assuming a rigid base. This difference is attributed to the flexibility of the baseplate connection.

a. internals of Test 4C attached to the vessel head for hammer impact tests

b. steel internal bolted to the earthquake simulator

Figure 10. Hammer tests for estimation of *in-air* natural frequency of different components

Table 2. Natural frequencies of various test components			
Component	Predicted frequency (FE model), Hz	Observed frequency (hammer test), Hz	Difference
Central steel internal (Test 2)	87.0	56.0	- 36%
Aluminum baffle (Test 2b)	130.0	130.0	0%
Steel plate (Test 3)	3.0	3.1	3 %
152 mm diameter internal (Test 4)	16.7	15.5	-7%
76 mm diameter internal (Test 4)	6.9	7.0	1%

5. Sample test results

5.1 Test 1

Figure 11 presents hydrodynamic response quantities and results from 1D theory [13] for unidirectional ECE input with a PGA = 0.8 g for the fixed-base (non-isolated) and isolated conditions. The difference in recorded and predicted peak responses, denoted ϵ, is presented in each panel.

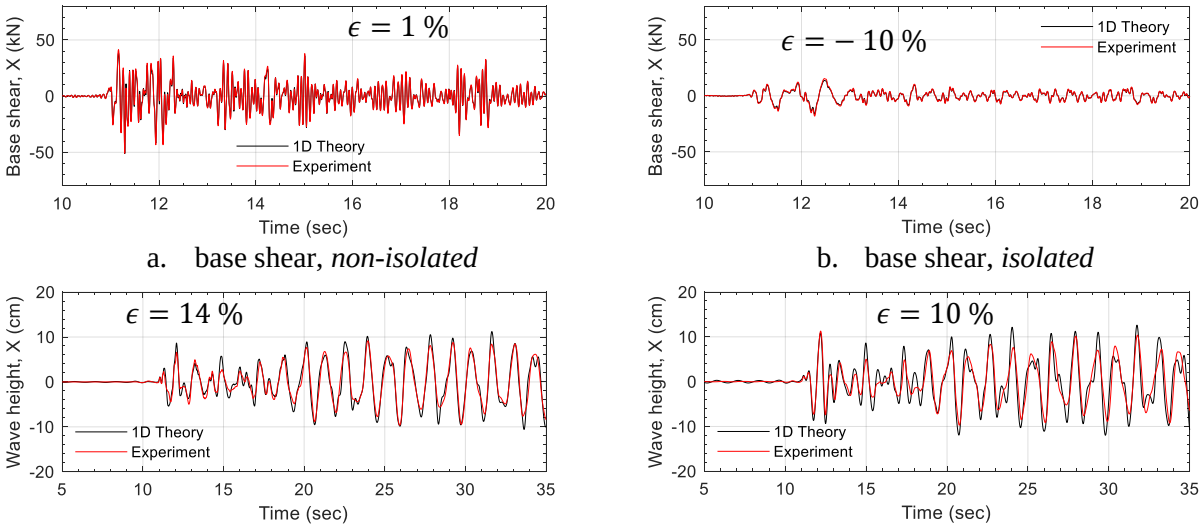

a. base shear, *non-isolated*
b. base shear, *isolated*
c. wave height, *non-isolated*
d. wave height, *isolated*

Figure 11. Hydrodynamic response histories for input motion ECE (PGA = 0.8g) and corresponding *isolated* motion for IS#1

Figure 12 enables a comparison of the peak hydrodynamic responses (pressure, base shear, base moment and wave height) obtained from tests using three unidirectional earthquake motions for the non-isolated and isolated conditions. The peak response for each isolated condition is normalized by the corresponding response for the *non-isolated* (fixed-base) input. There is a significant reduction in hydrodynamic pressure, base shear and base moment with an increase in the sliding period of the isolation systems (from IS#1 to IS#3). The effect of seismic isolation on wave height is not significant for this vessel and the chosen isolated periods.

Hydrodynamic responses in two orthogonal directions (x and y) are shown in Figure 13 for three-directional ECE input. Predictions of response based on 1D theory and the measured seismic inputs are included in each sub-figure. The percentage difference in peak response (ϵ) is identified. The use of 1D theory in this case recovers hydrodynamic responses reasonably well.

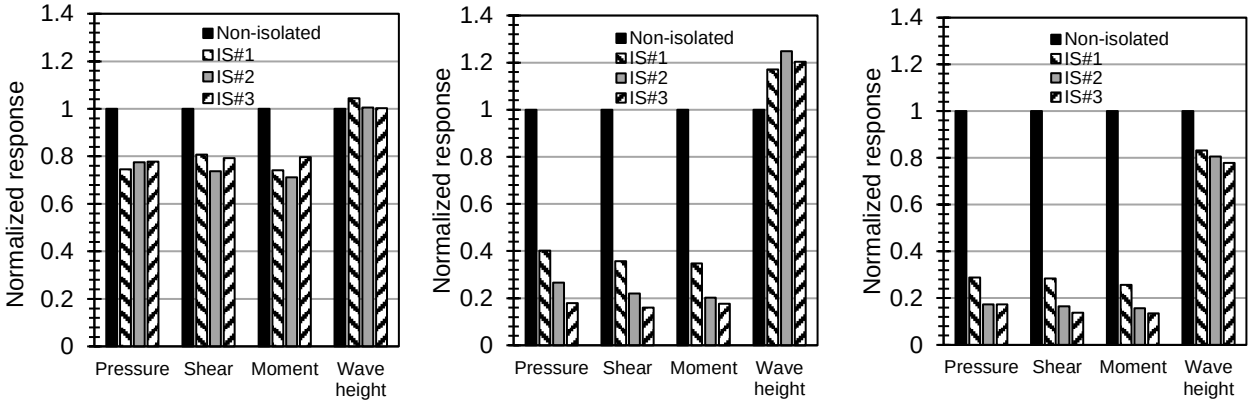

a. CCE (PGA = 0.1g) b. ECE (PGA = 0.8g) c. KCE (PGA = 0.8g)

Figure 12. Peak hydrodynamic responses recorded for the three isolation systems normalized by *non-isolated* (fixed-base) response

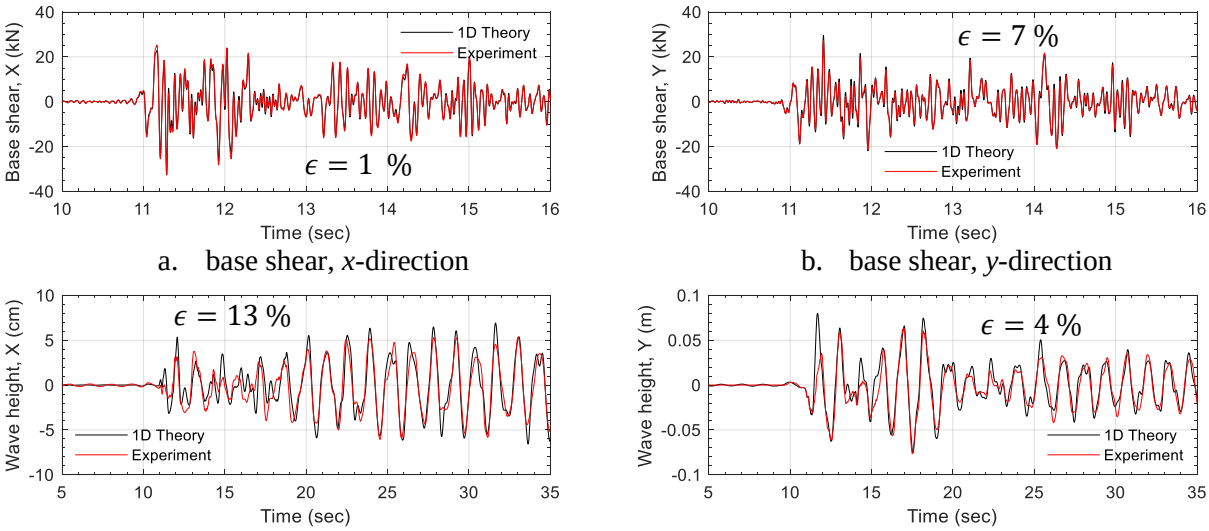

a. base shear, *x*-direction b. base shear, *y*-direction

c. wave height, *x*-direction d. wave height, *y*-direction

Figure 13. Hydrodynamic response histories for *x* and *y* directions for three-directional ECE input motion (*x*: 0.5g; *y*: 0.375g; *z*: 0.31g)

Hydrodynamic pressure histories from three pressure gages installed at different heights on the wall of the vessel are shown in Figure 14 for configuration B of Test 1 for unidirectional ECE input for the non-isolated and isolated conditions. The recordings from the three gages are virtually identical as is expected when sloshing is prevented. The significant reduction in pressure enabled by isolation is evident.

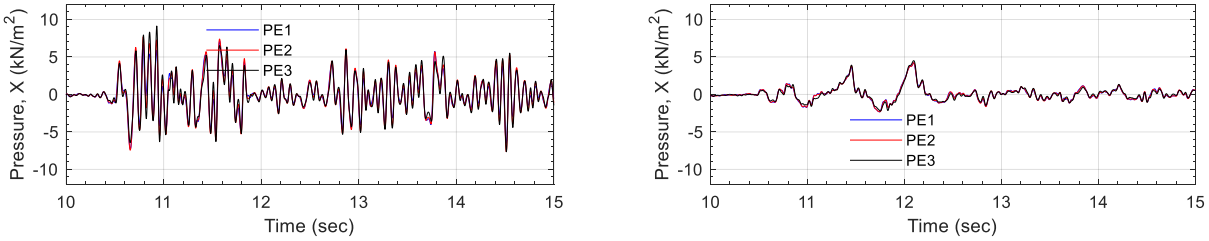

a. hydrodynamic pressure, *non-isolated* b. hydrodynamic pressure, *isolated*

Figure 14. Hydrodynamic pressure histories from pressure gages at 0.3 m (PE1), 0.9 m (PE2) and 1.5 m (PE3) above vessel base for ECE input motion (PGA = 0.8g) and corresponding *isolated* motion for IS#1

5.2 Test 2

Figure 15 presents pressure histories on the central steel internal (Test 2a) for three input motions for the non-isolated and isolated (IS#1) conditions. The recorded peak pressure for the isolated condition is expressed as a fraction of the recorded peak value for the *non-isolated* condition, denoted *r*, and presented in each sub-figure. The reduction in the pressure due to isolation is significant for the ECE and KCE inputs. For the CCE ground motion, the reduction is small because of its low amplitude and frequency content.

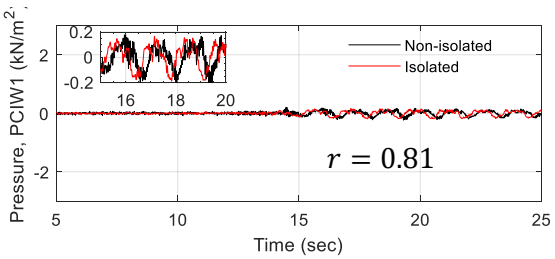

a. CCE (PGA = 0.1g)

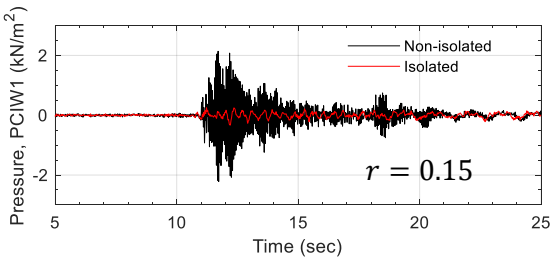

b. ECE (PGA = 0.8g)

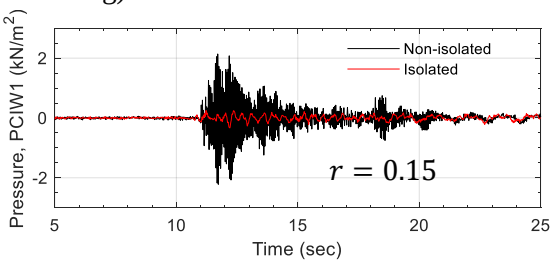

c. KCE (PGA = 0.8g)

Figure 15. Hydrodynamic pressure histories on the central steel internal for *non-isolated* inputs and corresponding inputs *isolated* using IS#1

5.3 Test 3

Figure 16 presents recorded acceleration histories for the steel plate (Test 3a) for three input motions for the non-isolated and isolated (IS#1) conditions. A significant reduction in acceleration in the isolated condition is observed for the ECE and KCE inputs, as expected. The increase observed for the CCE input is also expected due to its frequency content, as noted previously.

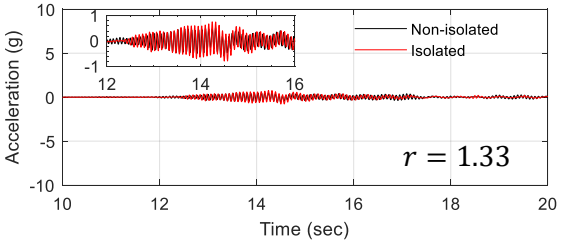

d. CCE (PGA = 0.1g)

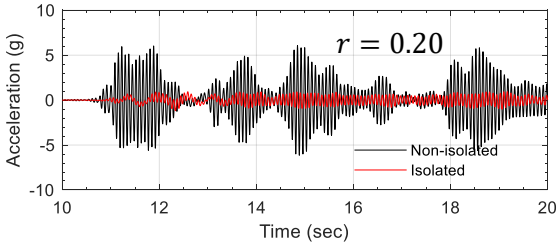

e. ECE (PGA = 0.8g)

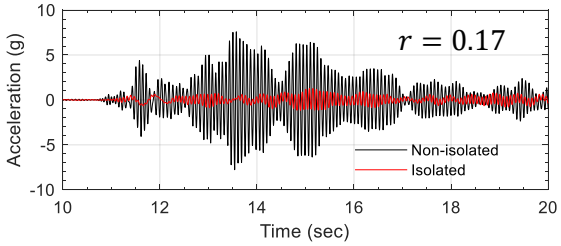

f. KCE (PGA = 0.8g)

Figure 16. Acceleration histories for the steel plate for the *non-isolated* and *isolated* IS#1 (conditions)

Snap-back tests were performed on the submerged plate to estimate its natural frequency and damping. The first mode frequency of the plate was estimated to be 2.07 Hz and 2.25 Hz in configurations A and B,

respectively, and the damping ratio was estimated to be 1.4% of critical in both cases. The different frequencies indicate different added masses for the plate in the two configurations. (The *in-air* frequency of the plate was estimated as 3.1 Hz (see Table 2) and the *in-air* damping was less than 0.1% of critical.)

5.4 Test 4

Acceleration and strain histories for the *non-isolated* and *isolated* conditions were recorded on the vessel and the internals for Tests 4A, 4B and 4C but are not presented here. Normalized power spectral density (PSD) plots of acceleration histories recorded from snap-back tests in water are shown in Figure 17. The added masses can be back-calculated from this information, noting that the *in-air* frequencies of the 152 mm and 76 mm diameter internals were 15.5 Hz and 7 Hz respectively (see Table 2). The coupling of responses is evident in the spectrum shown in Figure 17d (Test 4C) where two peaks are observed in the PSD of the acceleration response of the 76 mm diameter internal indicating that its response is affected by the vibration of the 152 mm diameter internal.

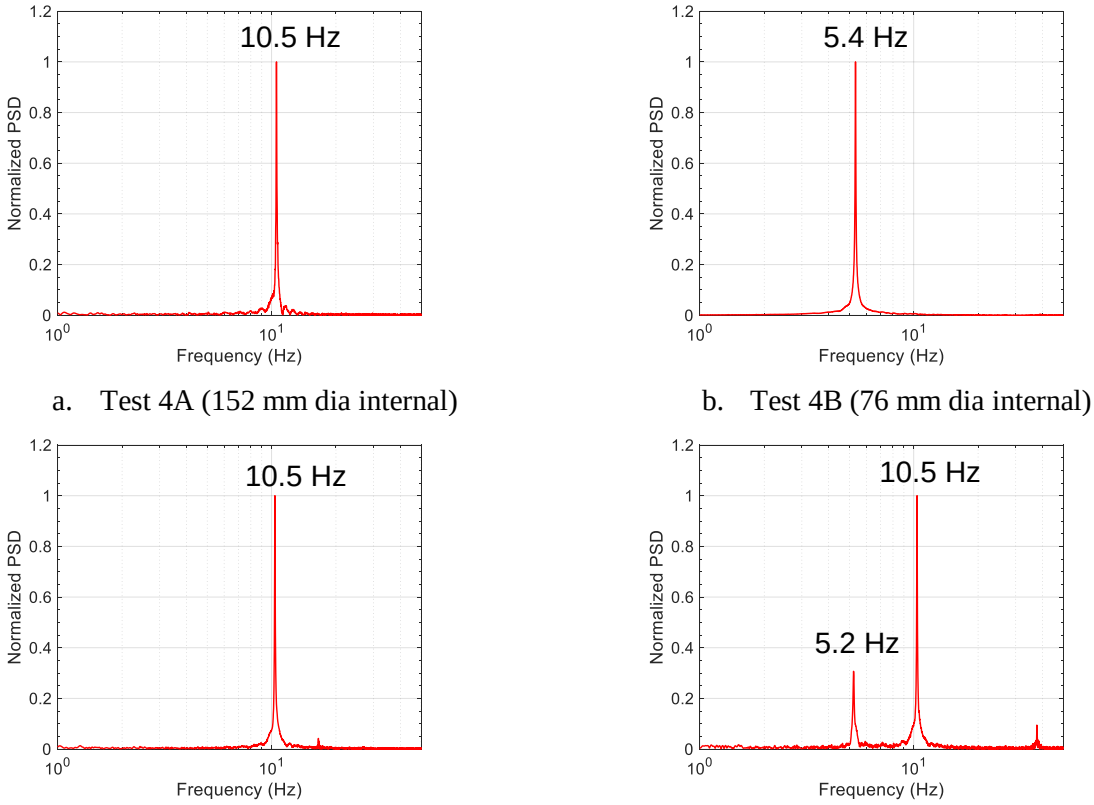

a. Test 4A (152 mm dia internal)

b. Test 4B (76 mm dia internal)

c. Test 4C (152 mm dia internal)

d. Test 4C (76 mm dia internal)

Figure 17. Snap-back test results for internals in Test 4

6. Closing Remarks

An experimental study on a 1/10th scale model of a base supported vessel with simplified representations of internals generated first-of-a-kind test data for multi-directional input motions under *non-isolated* and *isolated* conditions. Selected details of the four tests in the Phase II testing program were presented in the paper. Sample results were presented for Tests 1 through 4. The benefits of seismic isolation of equipment, measured here in terms of reduced pressures and base reactions on the vessel, and peak accelerations (and strains) experienced by a component, were demonstrated using numerically generated *isolated* inputs. The data generated from these test will be used for validation of numerical models in LS-DYNA and will be archived on DesignSafe [7] for future use by analysts.

7. Acknowledgments

The information, data, or work presented herein was funded by the Advanced Research Projects Agency-Energy (ARPA-E), U.S. Department of Energy, under Award Number DE-AR0000978. The views and opinions of the authors expressed herein do not necessarily state or reflect those of the United States Government or any agency thereof.

8. References

[1] Gluekler, E. L. (1997). "U.S. advanced liquid metal reactor (ALMR)." *Progress in Nuclear Energy*, 31(1- 2), 43-61.

[2] Mir, F. U. H., Yu, C.-C., Cohen, M., Bardet, P., Coleman, J., and Whittaker, A. (2019). "Dataset generation for validation of fluid-structure interaction models." *Transactions, 25th International Conference on Structural Mechanics in Reactor Technology (SMiRT-25)*, Charlotte, NC.

[3] Mir, F. U. H., Yu, C.-C., Charkas, H., and Whittaker, A. (2020). "Validation of numerical models for seismic fluid-structure interaction analysis of advanced reactors." *Proceedings, 2020 International Congress on Advances in Nuclear Power Plants (ICAPP 2020)*, Abu Dhabi, UAE.

[4] Yu, C.-C., Whittaker, A. S., Coleman, J. L., and Cohen, M. (2018). "Verification of a fluid-structure-interaction model for seismic analysis of Gen IV nuclear power plants." *Proceedings, 11th National Conference in Earthquake Engineering (11NCEE)*, Los Angeles, CA.

[5] Yu, C.-C., Mir, F. U. H., Cohen, M., Coleman, J., Bardet, P., and Whittaker, A. S. (2019). "Verification of numerical models for seismic fluid-structure-interaction analysis of advanced reactors." *Transactions, 25th International Conference on Structural Mechanics in Reactor Technology (SMiRT-25)*, Charlotte, NC.

[6] Yu, C.-C., Mir, F. U. H., and Whittaker, A. S. (2020). "Verification of numerical models for seismic fluid-structure interaction of advanced reactor internals." *Proceedings, 17th World Conference on Earthquake Engineering (17WCEE)*, September 2020, Sendai, Japan.

[7] Rathje, E. M., Dawson, C., Padgett, J. E., Pinelli, J. P., Stanzione, D., Adair, A., Arduino, P., Brandenberg, S. J., Cockerill, T., Dey, C., Esteva, M., Haan Jr., F. L., Hanlon, M., Kareem, A., Lowes, L., Mock, S., and Mosqueda, G., (2017). "DesignSafe: New cyberinfrastructure for natural hazards engineering." *Natural Hazards Review*, 18(3).

[8] Computers and Structures Incorporated (CSI) (2019). Computer Program SAP2000 (Version 20.2.0). Berkeley, CA.

[9] Malhotra, P. K., Wenk, T., and Wieland, M. (2000). "Simple procedure for seismic analysis of liquid-storage tanks." *Structural Engineering International*, 10(3), 197-201.

[10] Malhotra, P. K. (2006). "Earthquake induced sloshing in tanks with insufficient freeboard." *Structural Engineering International*, *16*(3), 222-225.

[11] Chalhoub, M. S., and Kelly, J. M. (1990). "Shake table test of cylindrical water tanks in base-isolated structures." *Journal of Engineering Mechanics*, 116(7), 1451-1472.

[12] Livermore Software Technology Corporation (LSTC) (2017). "LS-DYNA keyword user's manual-Version R 10.0." Livermore, CA.

[13] Yang, J. (1976). "Dynamic behavior of fluid-tank systems." Thesis, presented to Rice University, Houston, TX, in partial fulfillment of the requirements for the degree of Doctor of Philosophy.

